Reaction of Singlet and Triplet Methylene with Ethene. A Multireference Configuration Interaction Study

Willi Reuter, Bernd Engels,* and Sigrid D. Peyerimhoff

Institut für Physikalische und Theoretische Chemie, Universität Bonn, Wegelerstrasse 12, D-5300 Bonn 1, Federal Republic of Germany *(Received: September 3, 1991; In Final Form: February 24, 1992)*

Large-scale multireference configuration interaction (MRD-CI) calculations in a flexible atomic orbital (AO) basis are employed to study the reaction of C_2H_4 with CH_2 in its first triplet and singlet state. The minimum energy path (MEP) of both reactions is calculated, and different mechanisms are discussed. To examine the possible participation of the singlet state in the overall reaction starting from the triplet channel and terminating in the singlet-state c-C_3H_6, various cuts through both hypersurfaces are calculated. It is found that favorable interconversion from the triplet to the singlet surface can only occur at large separations of the two fragments of CH_2 and C_2H_4. Experimental data considering the vibrational motion of CH_2 in connection with the relative position of both surfaces are used to obtain an estimate for the overall barrier of the reaction. The height of the barrier is about 6 kcal/mol, while the barrier of the pure triplet reaction is calculated to be 7–9 kcal/mol.

Introduction

The chemistry of methylene, the simplest of the carbenes, is characterized by its two lowest states X $^3B_1(^3CH_2)$ and a $^1A_1$-($^1CH_2$) separated by ≈9 kcal/mol, which is an amount of energy easily accessible in chemical reactions. The electronic configurations are $(1a_1^2 2a_1^2 1b_2^2 3a_1^1 1b_1^1)$ for the triplet ground state and $(1a_1^2 2a_1^2 1b_2^2 3a_1^2)$ for the first singlet state. The $1b_1$ orbital will be called the π orbital of methylene while $3a_1$ will be called the σ orbital. The characterization of $3a_1$ and $1b_1$ as σ and π is justified by the fact that the $3a_1$ orbital lies within the plane of the molecule and contributes to σ bonds where as the $1b_1$ orbital is oriented perpendicular to that plane.

It is known[1] that the reactions of the molecule in the two states with olefins are quite different.

(a) The reactions of $^1CH_2$ are stereospecific additions toward an olefinic double bond. It consists of only one step. The reaction occurs without any Arrhenius activation energy. In competition there is the formation of propene via vibrationally excited species formed in the course of the reaction.

(b) The reaction of $^3CH_2$ with olefins must be divided into two major steps: first, the addition of $^3CH_2$ to the olefin, resulting in a triplet biradical. For the reaction of methylene with ethene this intermediate compound is called triplet trimethylene, hereafter referred to as ^{3}TM. The second step consists of an intersystem crossing from the intermediate compound to the singlet state of the final product. The lifetimes and properties of the intermediate compound characterize the final product. Therefore, reactions involving the $^3CH_2$ state are in general less stereoselective than those of the singlet state.

In a recent paper, Böhland et al.[2] studied the gas-phase reaction of $^3CH_2$ with ethene and several hydrocarbons over a wide temperature range. The experimental setup of Böhland et al. consisted of a discharge flow system and a photolysis cell for producing $^3CH_2$ from ketene by use of an excimer laser. A laser magnetic resonance (LMR) spectrometer and an additional UV resonance absorption device were coupled to the flow system. The LMR device was used for monitoring $^3CH_2$, whereas the UV device was used for monitoring the atomic species. For the reactions with hydrocarbons, they found a linear correlation between the activation energy of the particular reaction and the CH bond dissociation energy of the hydrocarbon under consideration. The activation energy increases with decreasing size of the hydrocarbon. For the two smallest homologues, ethane and methane, they found deviations from this correlation, which becomes more enhanced from ethane to methane. Since the activation energy needed for those reactions is of similar magnitude as the singlet–triplet gap of methylene, they postulated a concurrent reaction path involving the singlet state of methylene. It consists of a triplet–singlet excitation within the methylene followed by the singlet-state reaction. A similar pattern was found for the methylene–ethene reaction in which the activation energy of the reaction was determined to be 5.3 kcal/mol. Also for this reaction the experimental data indicate a participation of the singlet state, but further information on the extent of the influence of the singlet reaction does not exist.

In order to obtain more insight into the possible reaction pathways and the assumed participation of $^1CH_2$ in the reaction mechanism, we performed large-scale configuration interaction (CI) calculations on the reactions of $^3CH_2$ and $^1CH_2$ with both C_2H_4 and C_2H_6. In this paper we report our results of the reactions with ethene while a subsequent paper[3] deals with those with ethane. For the discussion of the concurrent mechanism $^3CH_2/^1CH_2$ + reactant, the shapes of the potential energy surfaces of the singlet and triplet reaction, in particular the barrier height along reaction pathways and the position relative to each other, are of interest.

The reaction of methylene with ethene was the topic of various theoretical studies. For the triplet-state reaction, most studies deal with the transition compound ^{3}TM itself or with the intersystem crossing from ^{3}TM to cyclopropane. For the first step of the reaction, i.e. the step of ^{3}TM formation, only a few studies are known.[4-6] In a MINDO/2 study, Bodor et al.[5] found the reaction to start with a symmetrical attack to the π bond. Along the reaction path the symmetry is lowered to C_s because $^3CH_2$ drifts away from the symmetric approach, forming the open chain ^{3}TM. The barrier of the reaction was calculated to be about 5 kcal/mol. Moreno et al.[6] used unrestricted Hartree–Fock (UHF) and Møeller–Plesset perturbation theory up to second order (MP2) involving a split-valence 3-21G basis set. They found a barrier between 4 and 11 kcal/mol, depending on the level of the treatment.

For ^{3}TM itself several studies also exist[7-11] in which either its geometry is optimized or the singlet–triplet crossing is calculated. The most sophisticated treatment from the theoretical point of view was that by Yamaguchi et al.[10] As in earlier work they found ^{3}TM to be a very floppy molecule.

The singlet-state reaction, $^1CH_2 + C_2H_4$, was the topic of various theoretical studies.[4,12,13] The most reliable treatment was used by Zurawski et al.[13] In this study the geometry optimization along the reaction path was performed on the self-consistent field (SCF) level involving a double ζ (DZ) basis set without polarization functions. At the geometries optimized in this manner, additional calculations were made in which correlation effects were included using coupled electron pair approximation (CEPA) and pair natural orbital CI (PNO-CI) treatments. Furthermore, the carbon basis set was enlarged by a d polarization function. A further discussion of the various studies will be given in comparison with our results.

The present paper is divided into four major parts. After a brief description of technical details, including a description of the basis set, geometry optimization strategy, etc., the singlet and triplet reactions will be discussed separately. In the third part the position of the two potential energy surfaces relative to each other is

0022-3654/92/2096-6221$03.00/0

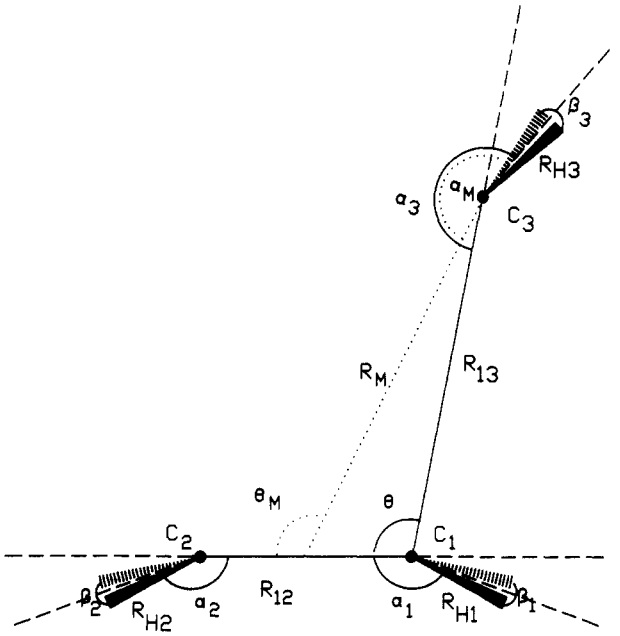

Figure 1. Structural parameters used for geometry optimization of the reaction of $CH_2 + C_2H_4$. The dotted lines show the parameters R_M, α_M, and θ_M chosen for the optimization of the singlet reaction. The numbering of the hydrogen centers is as follows: H_1, H_2 are connected to C_1; H_3, H_4 are connected to C_2; H_5, H_6 are connected to C_3; For the carbon–hydrogen distances the following abbreviations are used: $R_{C_1H_1} = R_{C_1H_2} \equiv R_{H_1}$; $R_{C_2H_3} = R_{C_2H_4} \equiv R_{H_2}$; $R_{C_3H_5} = R_{C_3H_6} \equiv R_{H_3}$.

studied. In the last section a possible participation of the singlet reaction is discussed.

Technical Details

The geometrical parameters used to describe both reactions of CH_2 with C_2H_4 are shown in Figure 1. The center C_3 refers to the methylene fragment whereas the centers C_1 and C_2 refer to the ethene fragment. The meaning of the parameters will be discussed in the next two chapters dealing with the minimum energy path (MEP) of the singlet and the triplet reactions.

The basis set employed in the calculations for both reaction surfaces was a standard Huzinaga (9s5p)[14] set of Gaussian type orbitals for the carbon atoms in a Dunning {4s2p} contraction.[15] An additional d function with an exponent of $\zeta = 0.7$ was introduced for proper description of polarization and correlation. For hydrogen the (5s) basis by Peyerimhoff et al.[16] was used in a {2s} contraction with a scaling factor of $\eta^2 = 2.0$. This basis set should provide somewhat better quality than a 6-31G* basis set.

The lowest occupied molecular orbitals (MOs) corresponding to the 1s orbitals of carbon were always kept doubly occupied in the CI calculations. In addition the same number of the highest virtual orbitals were discarded. So there are a total of 18 electrons which may be distributed among 54 orbitals for correlation by CI.

The CI calculations for the reaction surface were of multireference (MRD-CI) type;[17] they were done with a medium size set of reference configurations chosen in an appropriate manner with respect to the "active space" (see below) for each reaction. The total configuration space arising from single and double excitations relative to these reference configurations was of the order of 10×10^6. For configuration selection, a standard threshold of 10 μhartrees with an increment of 5 μhartrees was chosen for both reactions in order to obtain comparable results. The resulting space of selected configurations was of the order of 10000. MRD-CI and estimated full CI energies were evaluated in the usual manner.[17]

To test the quality of the calculations in describing the singlet–triplet gap, test calculations for the CH_2 fragment were performed. For $^1CH_2$ the length of the CH bond was determined to be 1.099 Å, whereas for $^3CH_2$ it was determined to be 1.072 Å. The HCH angle was calculated to be 103° for the singlet and 131° for the triplet. In their benchmark calculations Bauschlicher et al.[18] used 132.7° and 1.079 Å as the bond angle and CH bond length for $^3CH_2$ and 101.3° and 1.112 Å as the bond angle and the CH bond length for $^1CH_2$. On the basis of the ab initio data from Comeau et al.,[19] Jensen et al. derived a valence angle of 133.9° and a CH bond length of 1.075 Å for $^3CH_2$ and a valence angle of 102.2° and a CH bond length of 1.11 Å for $^1CH_2$ from experimental data.

TABLE I: Summary of the Calculations for Testing the Quality of AO Basis Set and One-Particle Basis

a. CH_2 Fragment

one-particle basis	estimated full CI (hartrees) $^3CH_2$	estimated full CI (hartrees) $^1CH_2$	triplet–singlet gap (kcal/mol)
$^1CH_2$–MOs	−37.0303	−37.0085	14
$^3CH_2$–MOs	−37.0305	−37.0085	14

b. $R_{13} = 2.5$ Å, $\theta = 116°$ (Geometries Optimized for $^3CH_2C_2H_4$)

one-particle basis	estimated full CI (hartrees) $^3CH_2C_2H_4$	estimated full CI (hartrees) $^1CH_2C_2H_4$	triplet–singlet gap (kcal/mol)
$^1CH_2$–MOs	−117.3268	−117.2884	24
$^3CH_2$–MOs	−117.3332	−117.2870	29

The energies of the test calculations are summarized in Table Ia using two different kinds of one-particle basis. The singlet–triplet splitting was calculated to be 31 kcal/mol at the SCF level. It decreases to 14–15 kcal/mol at the MRD-CI level and to 13–14 kcal/mol at the estimated full CI level. In what follows we will always refer to the estimated full CI energies which differ only slightly from the MRD-CI level of treatment. Summarizing, one can say that the singlet–triplet gap is overestimated by about 4–5 kcal/mol irrespective of which kind of one-particle basis, singlet MOs or triplet MOs, is used. The difference of 13–14 kcal/mol is in accord with the review of Shavitt,[20] where a splitting of 12–14 kcal/mol is cited for basis sets of double ζ plus polarization quality and CI-level treatment.

The dependence on the one-particle basis increases as the fragments CH_2 and C_2H_4 approach each other. In Table Ib, the calculation for $R_{13} = 2.5$ Å is given. The various geometrical parameters are defined in Figure 1. In this case the geometry of the supermolecule is optimized for the triplet state, so that the singlet–triplet gap at this geometry is much larger than that corresponding to the two optimal geometries. As expected the calculated singlet–triplet $CH_2C_2H_4$ gap is lowered by about 5 kcal/mol if singlet MOs instead of triplet MOs are used as the basis for the CI calculation. This difference can be divided into a raising of the triplet surface by about 4 kcal/mol (due to the less adequate singlet MO basis) and a lowering of about 1 kcal/mol of the singlet surface (as a result of the more appropriate MO basis). The difference between the two one-particle basis sets decreases to about 1–2 kcal/mol as CH_2 approaches closer to C_2H_4 ($R_{13} \leq 2.5$ Å). Because error cancellation occurs if singlet MOs are employed, they were taken to perform the CI calculations of both hypersurfaces. From this consideration the error in the singlet–triplet separation is estimated to be of the order of at most 4–5 kcal/mol. For better agreement with the experimental singlet–triplet splitting of $T_0 = 8.998$ kcal/mol and $T_e = 9.215$ kcal/mol,[19] the basis set has to be augmented up to a size impractical (or at least quite expensive) for calculations of a nine-center system.[18-20]

The optimization of the various geometrical parameters was performed in a two-step procedure. In the following chapter all parameters except the reaction coordinates R_{13} and θ will be called secondary geometry parameters. The optimization for the entire surface for the singlet and triplet reaction was done with the UHF-SCF gradient from the GAUSSIAN program package.[22] For both minimum energy paths (MEP), a grid optimization at the CI level was performed for the subset of the most important parameters. This subset consists of R_{12}, R_{H3}, α_1, α_2, α_3, and β_3.

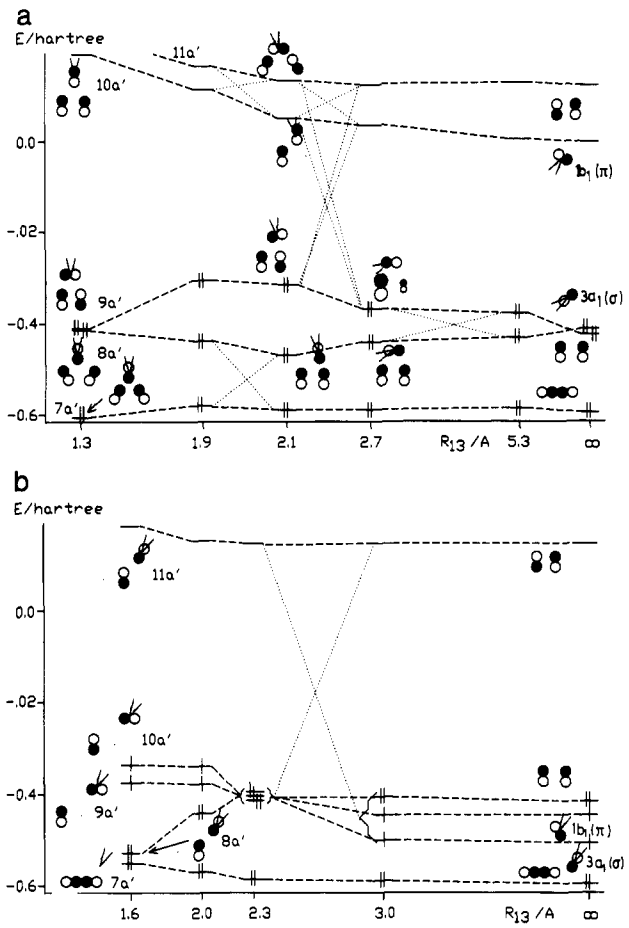

Figure 2. Orbital correlation diagrams for the occupied orbitals and the two lowest virtual orbitals of the reaction (a) $^1CH_2 + C_2H_4$ and (b) $^3CH_2 + C_2H_4$.

All remaining parameters which were determined in the first optimization step were relaxed in the course of the grid optimization if necessary. For the search for the singlet reaction MEP, a modified set of parameters (see Figure 1, dotted line) was used with θ_M, α_M, and R_M relative to the middle of the CC bond of the ethene fragment.

A crucial point for the participation of the singlet state in the reaction mechanism is the barrier height of the triplet reaction. To get a better description, several calculations with more sophisticated treatment were performed for the points R_{13} = 40.0, 3.0, and 2.3 Å of the triplet MEP. Details of these treatments will be given within the text.

Minimum Energy Path for the Reaction $^1CH_2 + C_2H_4$

For the symmetry forbidden C_{2v} or least motion attack, at least two configurations are necessary to describe the reaction path in a proper way. By symmetry breaking, this avoided crossing is reduced in the lower C_s group to crossings at the MO level resulting in one main configuration. The "active space" of this reaction is built up from the σ_p, π, σ_p^*, and π^* orbitals from ethene and the σ and π orbitals of CH_2 (see the MO correlation diagram, Figure 2). The rotation of the attacking CH_2 forces orbital mixing, causing the reaction to become allowed in terms of the Woodward–Hoffmann rules and decreasing the barrier caused by orbital crossings.

In the present work the energy at the estimated full CI level was calculated to be −117.3204 hartrees for the educts ($^1CH_2 + C_2H_4$ supermolecule at R_M = 40.0 Å) and −117.4850 hartrees for the product cyclopropane. The energy difference between reactants and product was determined to be ΔE = 103 kcal/mol, which is in good agreement with the heat of formation of ΔH_f = 102 kcal/mol[23,24] for this reaction (Figure 3).

For the singlet reaction the path of approach determined by Zurawski et al.[13] was taken as a first guess which had to be refined

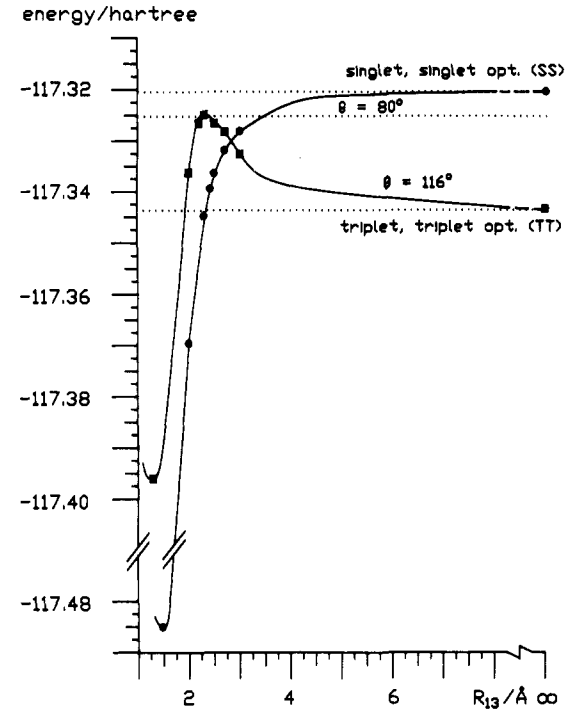

Figure 3. Potentials for the reactions of $^1CH_2 + C_2H_4$ and $^3CH_2 + C_2H_4$ along the minimum energy path. The dotted lines indicate (from top to bottom) the energy of the singlet channel, the energy of the barrier along the triplet MEP, and the energy of the triplet channel.

due to the lack of polarization functions on the carbon atoms in the earlier work. A grid optimization of the most important structural parameters at the CI level shows, however, that there are only slight deviations from the MEP determined by Zurawski et al. (Figure 4a). The changes in the optimal values of the parameters R_{12}, β_3, R_{H3}, α_1, and α_3 during the approach of CH_2 to the C_2H_4 are given in Figure 5a–e. Whenever reference to Figure 5a–e is made, it should be kept in mind that $R_{13} = [R_M^2 + {}^1/_4R_{12}^2 - R_MR_{12}\cos(180° - \theta_M)]^{1/2}$ is approximately equal to R_M for larger separations of the fragments. The CC bond R_{12} changes from 1.314 Å for large distances R_M (R_{13}) to $R_{12} = R_{13}$ = 1.514 Å at equilibrium geometry. The major changes are observed for $R_M \leq 2.1$ Å ($R_{13} \leq 2.0$ Å, Figure 5a). In this region the sp^2 hybrid changes into an sp^3 hybrid, as can be seen by the changes in α_1 (Figure 5d) and R_{12} (Figure 5a). The change in hybridization starts somewhat later at the C_2 carbon atom rather than at the C1 center. For $R_M \leq 1.9$ Å or $R_{13} \leq 2.0$ Å (the CH_2 fragment has a final orientation with $\alpha_M = 180°$ and $\theta_M = 90°$), the two carbon atoms C1 and C2 of the ethene fragment are equivalent again, as can be seen from the fact that $\alpha_1 = \alpha_2 = 160°$. The CH bond length R_{H3} (Figure 5c) varies rapidly and has shortened to the equilibrium bond length of 1.075 Å for R_M = 1.9 Å (R_{13} = 2.0 Å). Beginning with $\beta_3 = 102°$, the HCH angle (Figure 5b) opens to $\beta_3 = 132°$ (nearly the valence angle of $^3CH_2$) at R_M = 1.9 Å (R_{13} = 2.0 Å), indicating a reorganization of the electronic structure (which will be discussed in terms of the molecular orbitals 8a′ and 9a′). For smaller distances R_M (R_{13}), the angle β_3 decreases. For the inclination angle α_M (Figure 5e) of the attacking methylene, a value of 78° at R_M = 2.1 Å (R_{13} = 2.0 Å) was observed. Hence the rotation of the methylene may occur at a later stage in the course of the reaction. Using an inclination angle $\alpha_M = 90°$, the estimated full CI energy is higher by about 20 kcal/mol. The methylene fragment is nearly parallel to the ethene fragment in the case of $\alpha_M = 78°$, allowing bonding overlap of the π orbital of the methylene and the π MO of the ethene. For $\alpha_M = 90°$, the methylene is in a perpendicular position with no bonding overlap between the two MOs. The orientation of CH_2 is essential for this reaction. From SCF calculations it seems that symmetry breaking alone (by leaving the perpendicular axes of attack) is insufficient to explain the lack of a reaction barrier. Only when the MO correlation is taken into account in

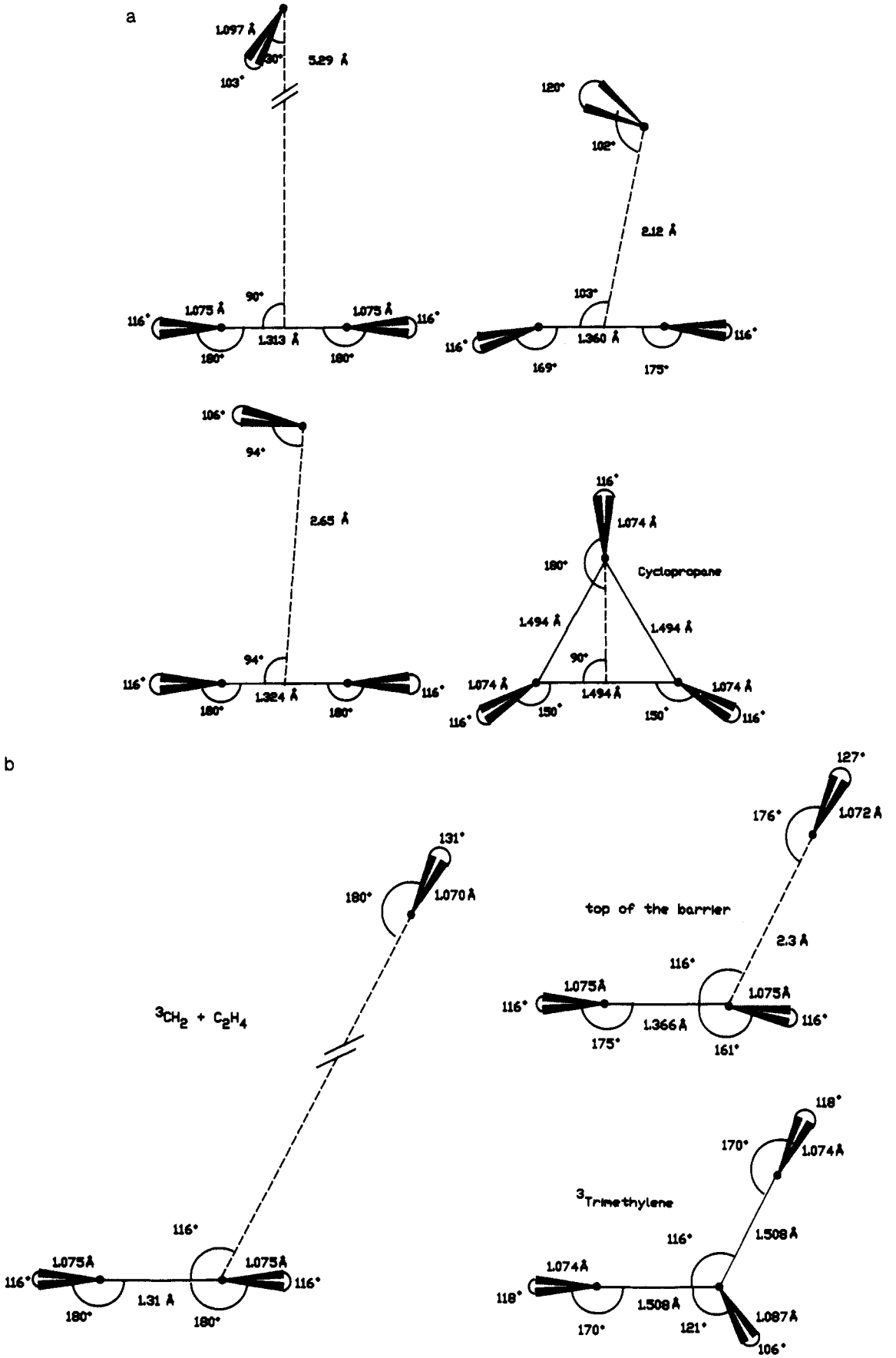

Figure 4. Particular geometries along the MEP of the reaction (a) $^1CH_2 + C_2H_4$ and (b) $^3CH_2 + C_2H_4$.

an appropriate manner does the reaction barrier disappear.

Due to the symmetry breaking effect of the CH_2 rotation, one carbon atom (C1) is attacked preferentially. This can be seen in the molecular orbital plots of the two highest occupied MOs (8a′ and 9a′ for small R_M or R_{13}; a_1 and π for large R_M or R_{13} values). A sketch of the MOs is given in the MO correlation diagram Figure 2a. At $R_M \geq 5.3$ Å ($R_{13} \geq 5.3$ Å) the positive linear combination (9a′) of the σ orbital of the methylene with

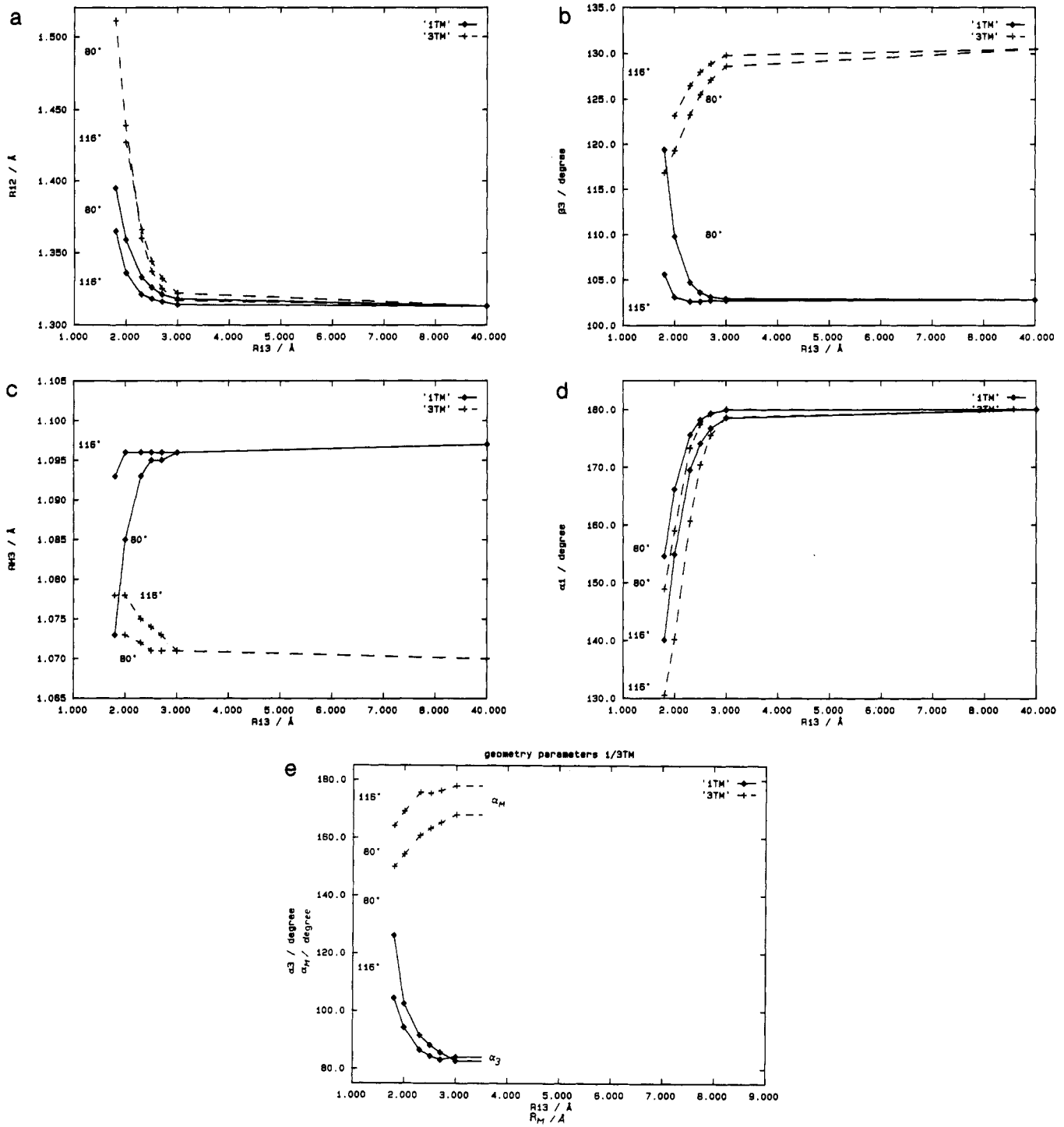

Figure 5. Variation of the structural parameters (^{1}TM/^{3}TM) with the intermolecular distance R_{13} for $\theta = 80°$ and $\theta = 116°$; (a) R_{12}, CC bond length of the ethene fragment; (b) β_3, HCH valence angle of the CH_2 fragment; (c) R_{H3}, CH bond length of the CH_2 fragment; (d) α_1, pyramidalization angle at carbon atom C1 of the ethene fragment; (e) α_3, inclination angle of the attacking CH_2 during the $^3CH_2 + C_2H_4$ reaction (this coordinate describes rotation of the CH_2 fragment for large distances R_{13}), of the ethene fragment, and α_M, inclination angle of the attacking CH_2 during the $^1CH_2 + C_2H_4$ reaction (this coordinate describes rotation of the CH_2 fragment for large distances R_M).

the π orbital of ethene is antibonding with a nodal plane between the two molecules. Due to the rotation of the CH_2 fragment in the course of the reaction, it turns into a strongly bonding orbital between CH_2 and C_2H_4. As a result stabilization of 9a′ occurs, so that between $R_M = 5.3$ Å ($R_{13} = 5.3$ Å) and $R_M = 2.7$ Å ($R_{13} = 2.7$ Å) the 9a′ orbital crosses with the 8a′ orbital, i.e. the two MOs exchange this character. From the point of view of the CH_2 fragment, it maintains its σ orbital character.

At $R_M \geq 5.3$ Å ($R_{13} \geq 5.3$ Å), the negative linear combination of the σ orbital of methylene and the π orbital of ethene form an MO with bonding overlap (8a′). The bond begins to form at the "hydrogen side" of the methylene. As discussed above, there is a crossing between 9a′ and 8a′, and at smaller R_M (R_{13}) separations, the original 8a′ character is now found in the 9a′ MO. In this region a bond begins to build between the C2 of ethene and the methylene C3. This MO is also responsible for the fact that for larger values of the angle θ (90°, 106°) the bonding behavior of the potential curve sets in at smaller R_M values. This behavior is understandable because the bonding between C3 and C2 is weakened if θ_M (θ) is enlarged, while at the same time the antibonding effect between C3 and C1 is strengthened.

As indicated by the different sizes of lobes of the π orbital 9a′ at $R_M = 2.7$ Å ($R_{13} = 2.7$ Å), mixing between the highest occupied orbital and the π^* orbital sets in very early in the course of the reaction. For values of $R_M \leq 2.7$ Å the mixing with the π^* orbital increases, and furthermore an interaction with the π orbital of

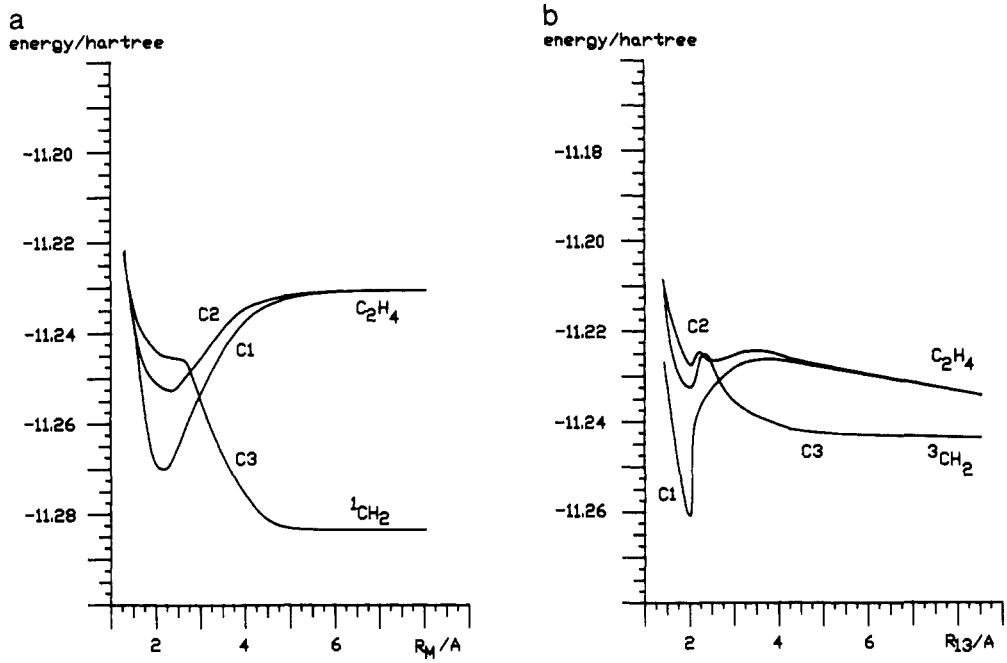

Figure 6. Canonical energies of the 1s orbitals for the reactions (a) $^1CH_2 + C_2H_4$ and (b) $^3CH_2 + C_2H_4$.

the methylene fragment starts (as indicated by the dotted lines in Figure 2a). The character of 9a′ has changed entirely at R_M = 2.1 Å, describing a bonding linear combination between the π^* of ethene and the methylene π. Also the HCH angle β_3 begins to open to its greatest magnitude of 132° (the same value as in triplet methylene) for a distance of R_M = 1.9 Å (R_{13} = 2.0 Å). Finally 8a′ and 9a′ contributes to the 3e′ orbital of cyclopropane. A similar feature was found by Ortega et al.[25] for the $^1CH_2 + H_2$ system.

The σ_p orbital of ethene shows mixing with the σ orbital of methylene in the last part of the reaction forming the $3a_2'$ orbital components of cyclopropane (7a′).

By symmetry the a″ orbitals cannot interact with the a′ orbitals. The a″ orbitals, which correlate with $1a_2'$ and 1e″ in cyclopropane, build three linear combinations. The major part describes the carbon hydrogen bonding, but the overall positive combination contributes to carbon–carbon bonding as well.

Using Koopmanns′ theorem,[26] the 1s orbital energies can be compared with the measured peaks of XPS (ESCA) spectroscopy.[27] It can be shown that the higher the inner-shell orbital energy the more negative are the surroundings of the atom under consideration.[28] An analysis of the orbital energies of the carbon 1s shell orbitals (Figure 6a) first shows an electrophilic phase of the reaction ($R_M \approx R_{13} \geq 2.1$ Å) followed by a transfer of charge density back to the ethene fragment during the formation of cyclopropane at smaller distances. The large difference of ≈50 mhartrees in the energies of the core orbitals of ethene and methylene is an indication of the electrophilic character of the methylene. It is seen from Figure 6a that during the first phase of the reaction the methylene core orbital is destabilized indicating charge accumulation around the methylene carbon atom. At the same time the core orbitals of the ethene carbon atoms are stabilized. The energy of the core orbital of the C1 atom is thus lowered more than the C2 core orbital. This is in accordance with the fact that the reaction follows an asymmetric approach in the first phase with preferred attack toward the C1 atom. All three core orbitals have nearly the same energy for $R_M \approx R_{13}$ = 2.8 Å where the descent of the CI surface starts (Figures 4a and 6a). For shorter distances the decrease of the orbital energies indicates a charge transfer back to the C1 and C2 atoms of the ethene fragment. By the penetration of methylene into the charge distribution of the ethene fragment, the core orbital of methylene is destabilized, indicating that the nucleophilic behabvior of the methylene is overcompensated at this stage of the reaction. Zurawski et al.[13] pointed out this two-phase mechanism as found by Kollmar[29] for the $^1CH_2 + H_2$ model. This two-phase mechanism was first postulated by Skell et al.[30] and supported by Hoffmann.[4]

Minimum Energy Path for the Reaction $^3CH_2 + C_2H_4$

For the optimized geometry of ^{3}TM (Figure 4b), the total SCF energy was determined to be −117.0016 hartrees while an estimated full CI procedure gives −117.3960 hartrees for this geometry. For the supermolecule $^3CH_2 + C_2H_4$ at R_{13} = 40.0 Å, the estimated full CI energy of −117.3435 hartrees was obtained. The energy difference between the reactants and the product is thus ≈33 kcal/mol at the estimated full CI level (Figure 3).

For the reaction of $^3CH_2$ with ethene along the axis with θ = 116° (along the MEP), SCF calculations yield an energy barrier near 24 kcal/mol. The top of the barrier lies at R_{13} = 2.3 Å.

Experimentally Böhland et al.[2] measured an activation energy of 5.3 kcal/mol at $T \approx 600$ K, giving a barrier of about 7 kcal/mol at T = 0 K, but it is unclear whether this is the barrier of the pure triplet reaction or if it is the activation energy of a reaction in which both the singlet and triplet take part. With inclusion of the correlation in the way as it was done for the entire surface the barrier on the triplet surface decreases to approximately 11 kcal/mol. As will be discussed later, the barrier height further decreases to about 7–9 kcal/mol if more sophisticated calculations are performed. The minimum of the potential energy surface of the triplet trimethylene (^{3}TM) was determined at a CC bond length of $R_{12} = R_{13}$ = 1.508 Å with a pyramidalization angle α_1 = 122° at carbon C1 (Figure 4b). The bond angle of the carbon skeleton of ^{3}TM is determined to be θ = 116°. The HCH angle β_3 of the attacking methylene decreases from 132° in the isolated fragment molecule to 107° in ^{3}TM. The symmetry of ^{3}TM is C_{2v} for the minimum geometry. Rotations of the terminal methylene groups cause energy differences of the order of 1 kcal/mol, while conserving C_{2v} symmetry. This optimized structure for ^{3}TM is in good agreement with the structures determined by Bodor et al.[5] who used MINDO/2 and Jean et al.[31] and Yamaguchi et al.[10] who employed two-configuration SCF calculations. Overall no more than 1 kcal/mol energy lowering should be expected for the fully optimized ^{3}TM.

The barrier region is easily identified due to the dramatic changes in the optimized parameters. The three most important parameters during the reaction are α_1, R_{12}, and β_3. The pyramidalization angle α_1 (Figure 5d) changes from 161° to 120° between R_{13} = 2.3 Å and the equilibrium structure (R_{13} = 1.508 Å). The major change happens between 2.3 and 1.8 Å. Analogous behavior is observed for the CC double bond of ethene (R_{12}), while the HCH angle β_3 does not show such abrupt changes (Figure

5b). The reorganization of the bonding situation at the C1 carbon from a planar sp^2 to a pyramidal sp^3 hybridized carbon in the last part of the reaction would require the choice of a parameter other than R_{13} as the reaction coordinate. A better choice of the reaction coordinate might be the pyramidalization angle α_1 or the C1–C2 distance R_{12}, both describing the change from sp^2 to sp^3 hybridization at the C1 center.

The orbital grouping for the triplet reaction is nearly the same as for the singlet reaction. Above the three 1s carbon orbitals there are the three 2s orbitals as a second group, each only building linear combinations within the respective subset. The next set consists of the σ_p, π, π^*, and σ_p^* of ethene and the σ and π orbital of methylene. For the triplet reaction the active space is built up from the π and π^* orbitals of ethene and the σ and π orbitals of methylene. The σ_p orbital of ethene experiences only minor perturbations by the σ orbital of methylene. A sketch of the active MOs is given in the MO diagram, Figure 2b.

Characteristic for the triplet reaction is the localization of the π and π^* orbitals into two p orbitals. In the course of the reaction the π (8a′) orbital of ethene combines with the σ (9a′) orbital of the methylene. For R_{13} = 2.3 Å, i.e. behind the barrier at the SCF level, the π^* (11a′) orbital interacts with all three highest occupied valence orbitals a_1 (8a′), b_1 (9a′), and π (10a′). From the mixing between π and π^* orbitals, single p orbitals localized at the ethene carbon centers are found. Both combine with the methylene σ and π orbitals resulting in the orbitals 8a′, 9a′, 10a′, and 11a′. This is accompanied by a large elongation of the R_{12} bond and the opening of the pyramidalization angle α_3, which indicate the broken double bond. In combination with the σ orbital of methylene, a bonding orbital similar to σ_p (7a′) is formed. This is the major part of the C1–C3 bond. The mixing between bonding and antibonding π orbitals can also be seen from the changes in the two open shells. In the process of the reaction, both methylenic orbitals gain greater contribution from the p orbital on C2. The 9a′ orbital in trimethylene may be called a bonding three-center π orbital because its bonding through space results from an overlap between the two terminal orbital lobes with antibonding character between the terminal carbons and the central atom. The 10a′ orbital is the corresponding antibonding orbital to 9a′. The orbital energy curves of these two orbitals undergo a crossing in the region of the barrier ($R_{13} \approx 2.3$ Å) which can be seen by focusing on the σ and π contributions from methylene. So the main π methylene component is found in the 9a′ of trimethylene.

The core orbitals exhibit nearly the same behavior for the methylene orbital as in the singlet reaction (Figure 6b). The C2 and C3 core orbitals are degenerate for trimethylene, as expected, with the orbital located at carbon atom C1 being stabilized by 0.03 hartree in the region about R_{13} = 2.0 Å, indicating charge deficiencies. For trimethylene there is also a reduced charge density around the C1 atom in comparison with the terminal atoms of trimethylene in its equilibrium geometry.

Moreno et al.[6] performed calculations on the reactivity of triplet carbenes using the GAUSSIAN 80 and GAUSSIAN 82 programs with the UHF formalism and a gradient optimization algorithm followed by Møeller–Plesset perturbation theory up to second order. The atomic orbital (AO) basis set used for the calculations was a split valence 3-21G without any polarization functions. The transition state obtained by Moreno et al.[6] differs from that obtained in the present work by a rotation of 90° of the attacking methylene around the axis of attack. The two hydrogen atoms of the methylene are coplanar to the three carbon atoms. For this conformation the virtual π MO of methylene can only interact in a nonbonding manner with the π system of ethene. The barrier changes from ≈4 to ≈11 kcal/mol at the UHF and MP2 levels, respectively. The difference between reactants and product is nearly the same at both levels of theory, 27 and 26 kcal/mol. Moreno et al.[6] obtained a charge transfer toward the methylene in agreement with the present interpretation of 1s orbital energies. A calculation performed for a geometry similar to the transition state of Moreno et al.[6] resulted in a slightly higher barrier for the triplet reaction. It seems that the addition of polarization functions and proper accounting for correlation is essential for a proper description of the energy differences of reactants and products.

Comparison between the Triplet and Singlet Reactions

Yamaguchi et al.[10] performed calculations on triplet and singlet trimethylene (^{3}TM and ^{1}TM; TT and TS case in our notation, see below) as well as for c-C_3H_6 using two-configuration SCF and SCF techniques. Their MC-SCF/SCF results for the energy difference between ^{3}TM and c-C_3H_6 is 34 kcal/mol, whereas our findings are 39 kcal/mol using CI-level calculations. This difference is not surprising if one considers that the singlet–triplet gap of CH_2 is reduced by 17 kcal/mol when taking into account that electron correlation lowers the singlet more than the triplet. Furthermore, Yamaguchi et al. found several conformers of ^{3}TM with energy differences of 1–2 kcal/mol relative to each other and the open chain ^{1}TM lying above the ^{3}TM at θ = 116°. This close energetic neighborhood of the two species ^{1}TM and ^{3}TM is confirmed by the present work which obtains ^{1}TM 5 kcal/mol below the optimized triplet structure. From this finding and the earlier work, one could draw the conclusion that ^{3}TM should easily show conversion onto the singlet hypersurface and form more stable products whenever it has reached the absolute minimum on the triplet hypersurface.

The reaction of $^3CH_2$ could be accelerated by participation of the singlet state if it were possible to circumvent the total triplet reaction barrier, so that a lower barrier results for the combined reaction. For the present study this could happen because the singlet dissociation channel is higher than the triplet channel, but in contrast to the triplet reaction no barrier is found on the singlet minimum energy path (MEP). The comparison of both MEPs given in Figure 4 could be a good example. A triplet–singlet intercombination at the crossing point of both states would lower the barrier height by a factor of 2 so that the reaction

$$^3CH_2 + C_2H_4 \rightarrow {}^3CH_2C_2H \rightarrow {}^1CH_2C_2H_4 \rightarrow \text{products} \qquad (1)$$

would be much faster than the pure triplet reaction.

In comparing both MEPs, however, one must remember that the geometries used for both calculations differ extremely (see above). Hence, the scheme given in eq 1 has to be modified to incorporate the effect of the change in geometry

$$\begin{aligned} ^3CH_2 + C_2H_4 &\rightarrow {}^3CH_2C_2H_4 \text{ (triplet geometry)} \\ &\rightarrow {}^3CH_2C_2H_4 \text{ (singlet geometry)} \\ &\rightarrow {}^1CH_2C_2H \rightarrow \text{products} \end{aligned} \qquad (2)$$

where the height of the additional barrier in going from the triplet to the singlet geometry affects the total barrier height considerably.

The situation is even more complicated as not only do the reaction coordinate R_{13} and the angle of attack θ differ for both MEPs, but all other geometry parameters which were collected into the set of secondary geometry parameters differ, as well. Single dependencies between the reaction coordinates R_{13} and θ and the secondary geometry parameters will be discussed below. To get an idea of the influence of secondary geometry parameters on the total energy, we calculated the singlet state along the MEP of the triplet state using the optimized geometry parameters of the triplet state. It was found (Figure 7b) that the section on the singlet hypersurface along these geometrical parameters is so high in energy that a crossing with the triplet state would not occur in the region of interest. The other possible crossing region which is obtained if the triplet is calculated with the geometries of the singlet state is expected to lie much lower. Therefore, it was necessary to optimize the singlet geometries along the triplet MEP.

A crossing could also occur somewhere on the potential energy surface (PE) along the reaction coordinates, i.e. in neither the optimal singlet nor the optimal triplet MEP. We therefore studied the approach to CH_2 to C_2H_4 for five different θ angles: 126°, 116°, 106°, 90°, and 80°. Plots of the energy cross sections for the different θ angles are given in Figure 7. For each θ, four different sections, two through the hypersurface of the $^3CH_2$ + C_2H_4 approach and two through the corresponding hypersurface of the singlet state, were calculated. One energy cross section contains the optimized secondary geometries of the given state,

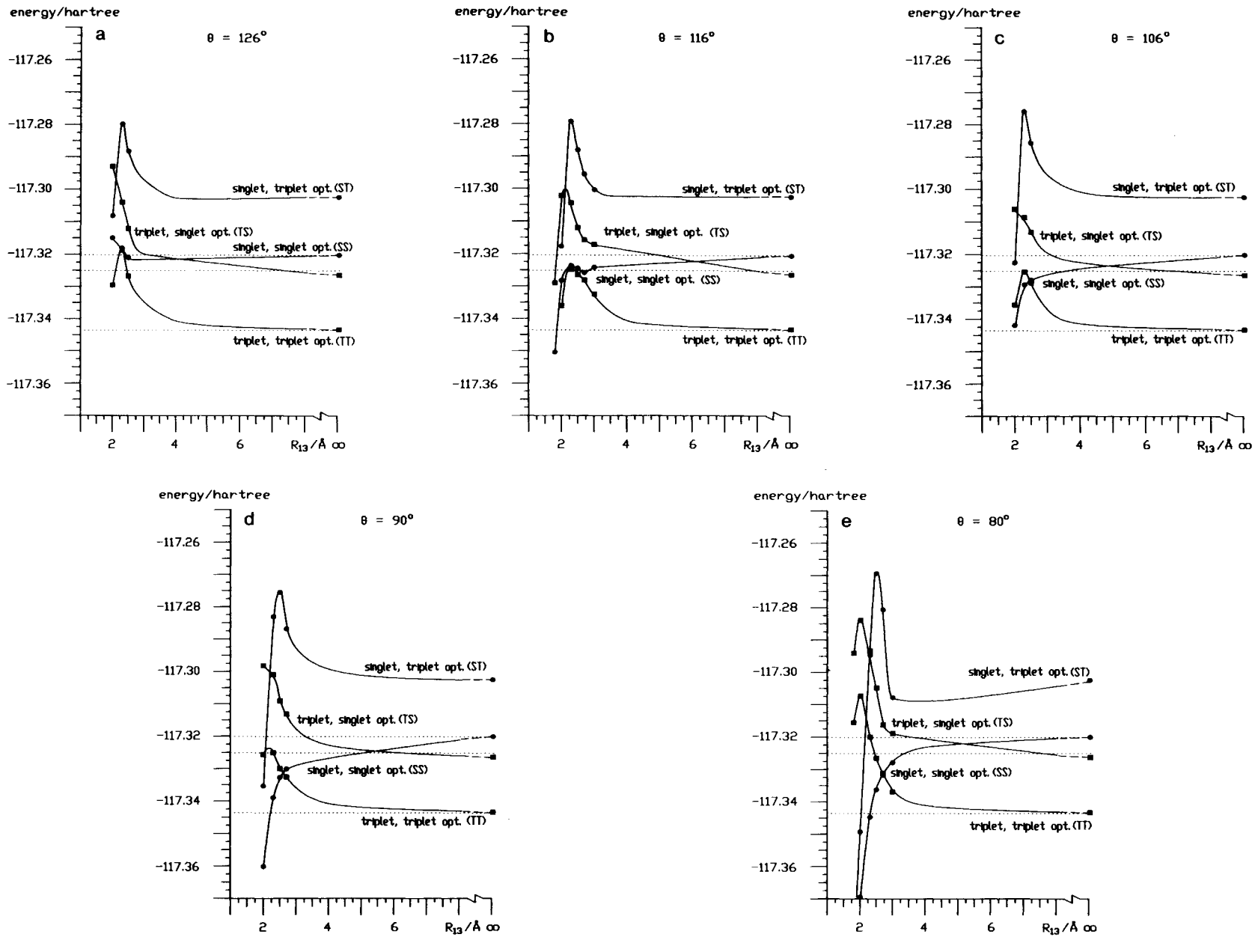

Figure 7. Energy cross sections for the angle θ: (a) $\theta = 126°$; (b) $\theta = 116°$; (c) $\theta = 106°$; (d) $\theta = 90°$; (e) $\theta = 80°$. The dotted lines indicate (from top to bottom) the energy of the singlet channel, the energy of the barrier along the triplet MEP, and the energy of the triplet channel.

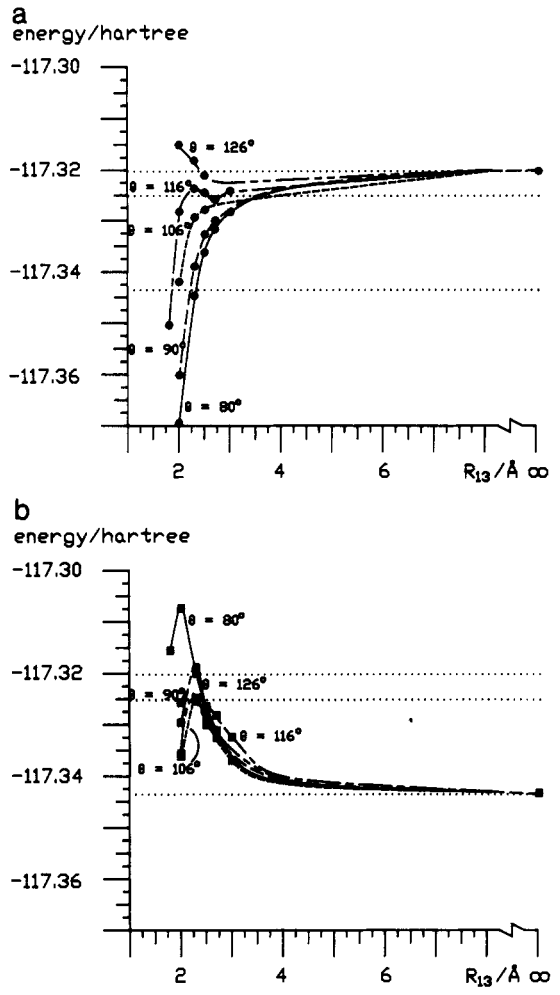

Figure 8. Comparison of the energy cross sections for the (a) triplet case for the angles θ = 126°, 116°, 106°, 90°, and 80°, and (b) singlet case for the angles θ = 126°, 116°, 106°, 90°, and 80°.

while the others were calculated with the secondary geometry parameters optimized for the other state. The two energy cross sections through the triplet hypersurface are marked with TT, indicating that the triplet state was calculated using its own optimized set of secondary parameters, and TS, which characterizes the triplet state calculated with the set of secondary geometry parameters optimized for the singlet state. The energy cross sections through the singlet hypersurface are characterized analogously with SS and ST. Most of the calculations were performed in the region of the triplet barrier because this is the most interesting part of the hypersurfaces since we are looking for a triplet–singlet intercombination. Because we expected no additional barrier on the reaction path to the products once the barrier is overcome, the energy minima for the individual curves at fixed θ angle were not calculated. An insight into the problem of the triplet–singlet crossing should be possible by comparison of the energy cross sections discussed above. Further barriers which are conceivable by varying the geometries from the triplet to the singlet are not obtained by this procedure, but the amount of computer time which would be required to test the entire multidimensinal surface did not seem to be justified.

An overview of the behavior of the TT cross section can be seen in Figure 8a, where a comparison of the various curves for fixed angles θ is shown. It is seen that the differences between the various curves are small for the angles θ of 116°, 106°, and 90°. The barrier height for all three approaches lies around 11 kcal/mol. From this we expect that the triplet reaction can easily occur in this range of θ values. Only approaches of CH_2 with θ = 80° or 126° are less favorable because the barrier height increases to 23 and 16 kcal/mol, respectively.

Furthermore the shape of the individual curves is very similar; only for θ = 116° is the barrier somewhat broader. For each curve the slope when coming from the dissociation channel is less steep than the descent to the minimum. The reason for the small differences between θ = 116°, 106°, and 90° lies in the nature of the ^{3}TM, which is a very floppy molecule.

The different SS curves are compared in Figure 8b. They show different behavior than the TT curves. No barrier is found for the attacks with θ = 80° (more or less the MEP of the singlet reaction) for those with 90° and 106°, but the descent to the minimum of the curves coming from the dissociation channel sets in much later, i.e. at smaller values of R_{13}. While for θ = 80° the descent already starts at R_{13} > 3.0 Å, for θ = 106° the energy first decreases after R_{13} = 2.5 Å. From this we expect that if the singlet hypersurface is reached from a triplet–singlet crossing at a different θ value, the successive reaction path of a singlet reaction would collapse to the θ = 80° cross section through the singlet hypersurface. Thus, barriers on the singlet hypersurface which appear for θ = 116° and 126° would be circumvented. Furthermore, the fact that each approach of $^1CH_2$ to C_2H_4 is expected to collapse to the MEP explains the unusually large preexponential factors found for the singlet reaction.[23] The strange behavior of the θ = 116° energy cross section between R_{13} = 3.0 and 2.5 Å was examined and it does not seem to arise as an artifact of the calculation. No further investigations were performed because this region is not very important for the overall singlet reaction path, as discussed above.

The reason for the behavior of the singlet hypersurface for varying the θ value is 2-fold. First, the absolute minimum C_3H_6 is quite deep. It lies about 35 kcal/mol below the minimum of the θ = 116° section. The reason for the differences between the singlet curves for different θ values is found in the reaction mechanism (Figure 2a). As discussed for the MEP of the singlet reaction for 3.0 Å > R_{13} > 2.5 Å, a bond is built between the methylene carbon center and the C1 carbon center of ethene. It has its origin in the overlap between the σ orbital of methylene and the π orbital of ethene. This bond is broken again for smaller R_{13} values due to the rotational motion of the methylene along the reaction path. The strength of this bond relies on the orientation between the two orbitals. It is weakened if θ is enlarged so that for larger θ values the descent to the minimum starts at smaller R_{13} values. The different behavior of the various curves for smaller R_{13} values can be reduced to the fact that the c-C_3H_6 lies about 35 kcal/mol below the minimum of the θ = 116° curve.

To study the possibilities for the participation of the singlet state in the total reaction, we will first examine the various energy cross sections for different θ values starting with θ = 116°, which is the optimal angle of attack for the pure triplet reaction. The calculated energy cross sections are shown in Figure 7b. Energetically the TT cross section is the lowest along the entire approach of CH_2 to C_2H_4; it corresponds to the MEP of the triplet reaction, as discussed in the previous section. The next curve at large CH_2 and C_2H_4 separations is the TS curve which describes the triplet state calculated with the set of secondary geometries optimized for the singlet state. Its dissociation limit lies about 10 kcal/mol above the dissociation channel of the TT curve, and its overall shape is similar to that of the TT curve but shifted to higher energy by about 8–13 kcal/mol. During the CH_2 approach it crosses with the SS curve somewhere between the dissociation limit and R_{13} = 3.0 Å. For the cross section through the singlet hypersurface the lowest energy (SS) was calculated to lie about 14 kcal/mol above the TT dissociation limit. This is equal to the calculated singlet–triplet splitting in CH_2, as discussed in the technical details. During the approach the energy decreases from R_{13} = 40.0 to 2.7 Å by about 3–4 kcal/mol. As discussed above (Figure 7b) between R_{13} = 2.5 and 2.0 Å a small barrier of about 1 kcal/mol in the SS curve has to be overcome before it descends to the minimum of the θ = 116° curve. Therefore, no crossing between SS and TT occurs. The ST curve (the calculation of the singlet state with the geometries of the triplet state) is so high in energy that it cannot participate in the reaction. This case will not be discussed any further.

The real crossing between the triplet state and the singlet state is given by a crossing between the TS and SS curves. As discussed

above, this occurs at large R_{13} values (3.0 Å < R_{13} < 40.0 Å). Since the interaction between the two fragments are small at large distances, experimental results for methylene in connection with the calculated behavior of the SS and the TT curve can be used to estimate the lower and upper energy bounds of the crossing. This is discussed further in the next section.

For θ = 106° and 90° (Figure 7c,d) both energy cross sections through the triplet surface, TT and TS, possess a very similar shape to that for θ = 116° in the region of interest around the TT barrier. Differences in the singlet curves result from the earlier descent (at larger R_{13} values) of the potential curve to the minimum. The crossing point between the TT curve and the SS curve therefore happens below the top of the triplet barrier, but one has to keep in mind that the geometries of both curves are different. The real crossing between the triplet-state and the singlet-state surface, given by the crossing between TS and SS curve, is less affected by changes in the SS curve. The energetical bounds of the crossing should not differ from those for θ = 116°. Small differences may arise since the descent of the singlet curve starts at larger R_{13} values.

For the remaining two θ values of 80° and 126° similar situations are also found (Figure 7a,e). Since both are more unfavorable for the triplet reaction, they are less important in the context of the triplet–singlet crossing. The curve for θ = 80° will only be important because it corresponds to the MEP of the pure singlet reaction.

A summary of the results of the calculations is as follows: Interconversions between the triplet and singlet states with barrier heights lower than 11 kcal/mol can occur only at large R_{13} distances (R_{13} > 3.0 Å). At smaller distances crossings are much higher in energy (ΔE > 20 kcal/mol). The calculations performed in the present work are not accurate enough (for further predictions, i.e. to determine the energy bounds for a possible crossing between 3.0 Å < R_{13} < 40 Å). Such calculations would require basis sets and theoretical methods much too costly for systems with nine nuclear centers since the energy differences between the various possible pathways are very small (less than 5 kcal/mol). However, as discussed above the calculations show that an estimate of the energy bounds can be obtained from experimental results considering the singlet–triplet splitting of methylene in connection with the calculated relative behavior of the TT and SS curves to one another. This is considered in the last section.

Possible Participation of the Singlet State

When nuclear motion is taken into account, a possible conversion from the triplet state to the singlet state can occur if two vibrational levels (or two rovibrational levels) of the two electronic states happen to coincide in energy. For a definite prediction of the energetic position of rovibrational levels, the error bars within the theoretical methods used in the present study are too large. However, the study shows that a favorable crossing can only occur at a large separation between the fragments CH_2 and C_2H_4, where their interaction is so small that only small perturbations of the single fragments are expected. This is supported by the findings that all secondary geometry parameters remain nearly constant between R_{13} = 40.0 and 3.0 Å. The most important geometrical parameter is β_3 which describes the bending vibration of the CH_2 fragment. Therefore a good estimate of the lower and upper energy bounds of a possible crossing can be obtained from experimental findings for the bending vibration of the methylene fragment in connection with the relative position of SS and TT curves to each other. The situation is sketched in Figure 9. On the left hand side the situation for infinite separation of the fragments is shown. There is no perturbation from C_2H_4 so that the singlet and triplet structures are determined only by the CH_2 fragment. The presented data are taken from a paper by Jensen et al.[19] who used the Morse oscillator–rigid bender internal dynamics operator (MORBID) to determine the rovibrational energy levels in CH_2. On the right hand side an estimate of the situation is given when both fragments are separated by about 3.0 Å. For this we assumed that the separation of the energy level in each state does not change, while the position of both electronic states

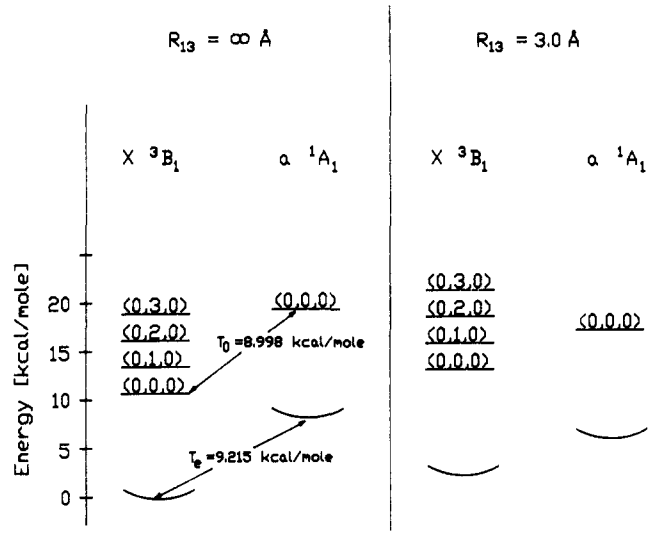

Figure 9. Estimate for the lower and upper energy bounds of the intersystem crossing taken from the experimental data of $^1CH_2/^3CH_2$ for infinite $C_2H_4 + CH_2$ separation R_{13} and for intermediate separation (R_{13} = 3.0 Å). (ν_1, ν_2, ν_3) are vibrational levels of CH_2. For more details see text.

relative to each other changes due to the approach of C_2H_4. The data for the shifts of the potential surfaces for both states are taken from our calculations. The triplet state is shifted to higher energies by 2 kcal/mol, while the energy of the singlet state is lowered by 2 kcal/mol. The conclusion from these considerations will be drawn after the discussion of the barrier of the pure triplet reaction.

While the energy bounds for the singlet participation can be taken from experimental data, this is not possible for the barrier height of the pure triplet reaction. In order to obtain more reliable data for this process, a series of additional calculations were performed for R_{13} = 40.0, 3.0, and 2.3 Å, varying the basis set size ([4s2p2d/2s], [4s2p2d/2s1p], [5s3p2d/2s1p]) as well as the number of configurations handled variationally. Furthermore, instead of canonical SCF orbitals the one-particle basis was obtained from CASSCF calculations using an active space of the four orbitals σ_p, σ_p^*, π, and π^* (see discussion of the triplet MEP). Regardless of the size of the basis set, the CASSCF calculations gave a barrier height of about 12–13 kcal/mol, which we assume to be too high. For the MRD-CI treatment two effects arise. If the basis set size is enlarged, the barrier height increases by about 3 kcal/mol, from ≈11 kcal/mol using the standard treatment ([4s2p2d/2s], SCF orbitals, T = 10 μhartrees) to ≈14 kcal/mol if the larger [5s3p2d/2s1p] basis set is employed in connection with CASSCF orbitals and a selection threshold of T = 10 μhartrees. Using the large basis set the barrier decreases to about 8–9 kcal/mol if the number of configurations handled variationally is increased from 12 000 SAF (selection threshold T = 10 μhartrees) to 32 000 SAF (T = 3 μhartrees). If besides the 1s shells of the carbon centers the $4\sigma_g$ shell of C_2H_4 is also kept doubly occupied, the selection threshold could be lowered to 2.0 μhartrees (remaining below 32 000 SAFs). In this case the barrier height stays around 8–9 kcal/mol. Using a more optimized one particle basis obtained by an increase of the active space within the CASSCF did not change the barrier height more than 0.5 kcal/mol at CI level. All CI energies above are estimated full CI energies.[17] If the higher excitations are estimated by an ACPF treatment[21] instead of the usual Davidson type procedure, no changes in the barrier height are found. Solving the problem by using a full MR-CI instead of a truncated MR-CI is not possible because the number of generated configurations is far beyond 10 × 10^6.

Taking into account the uncertainties in the estimation of the contribution of the nonvariationally handled configurations and deficiencies in the AO basis set size, our best estimated guess for the barrier of the pure triplet reaction is around 7–9 kcal/mol. Even though the actual size of the barrier height is influenced in a quantitative manner by the accuracy of the treatment, we

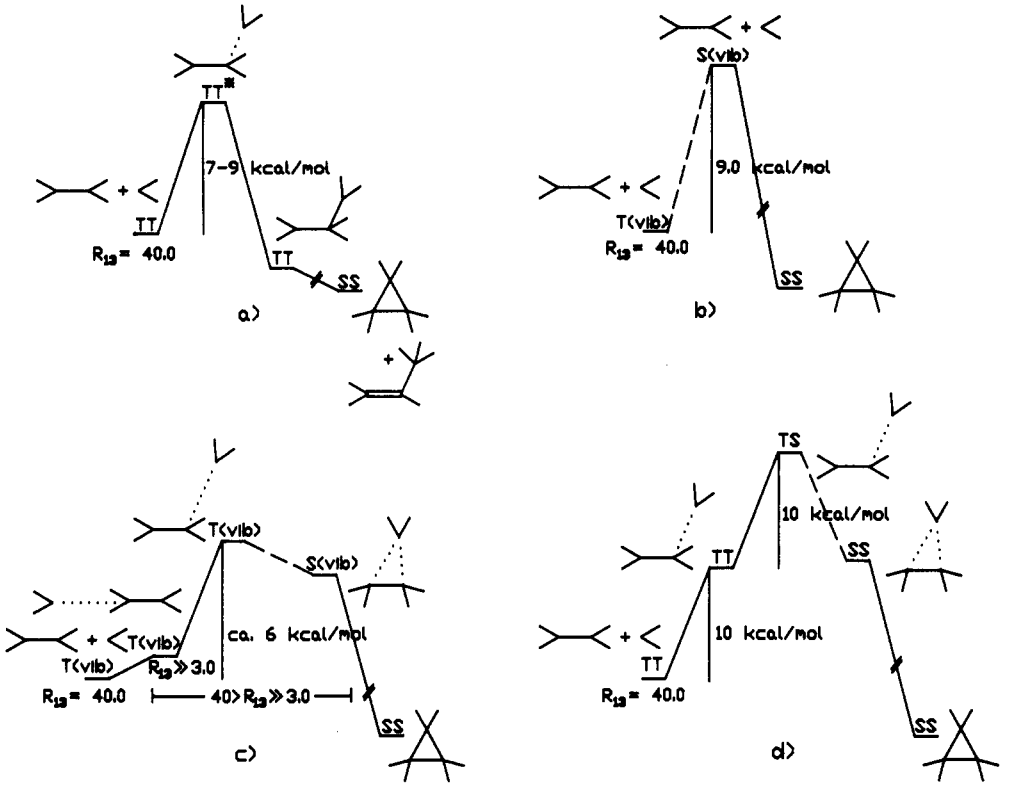

Figure 10. Possible mechanisms for the singlet–triplet crossing (distances given in angstroms): (a) crossing at the minimum of the ^{3}TM; (b) crossing at very large distances ($^3CH_2 \rightarrow {}^1CH_2$); (c) crossing in the region of weak CH_2–C_2H_4 interaction; (d) crossing at the barrier of the triplet reaction.

expect that the qualitative features of the triplet and singlet surface will not change if more sophisticated treatments are used. With this and the data presented in Figure 9, we are able to discuss several possible pathways.

The four important reaction pathways for the present problem are sketched in Figure 10. All start from the TT channel and terminate at the c-C_3H_6 molecule. The first extreme possibility is shown in Figure 10a. The reaction path goes along the pure triplet reaction path climbing over a barrier which was calculated to be about 7–9 kcal/mol. The triplet–singlet crossing occurs from ^{3}TM and was discussed in several earlier studies.[10,31] We can deduce from the present work that for this approach the energy barrier is very similar for the region of θ between 116° and 90°. For Figure 10a (and Figure 10d below) the electronic energy data are sufficient, because an estimate of the zero point energies for the entire system at infinite separation and at the top of the barrier (using the GAUSSIQN 86 program package[22]) shows only small differences.

In the second extreme possibility of singlet participation, the triplet–singlet crossing already occurs in the CH_2 fragment (Figure 10b). In the discussion of Figure 10b,c, the vibronic structure has to be taken into account. In Figure 10 this is indicated by T(vib) (vibrational state of the triplet) and S(vib) (vibrational state of the singlet). Using the experimental singlet–triplet gap of methylene (Figure 9), the barrier which has to be overcome is equal to the energy difference between the two lowest vibrational levels of the singlet and the triplet state, which was given as about 9.0 kcal/mol by Jensen et al.[19] This is nearly as high as the barrier of the pure triplet reaction path. After that, the reaction runs along the singlet surface on which no further barrier exists. Of course all θ values possess the same activation energy because during the singlet reaction an alignment of the CH_2 occurs. As discussed above the reaction path will collapse to the MEP of the singlet reaction.

The third path, shown in Figure 10c, describes a compromise between the two extreme possibilities. The interconversion from the triplet surface to the singlet surface occurs somewhere between infinite separation and R_{13} = 3.0 Å. The energetic upper bound is given by the situation at infinite separation which is equivalent to the singlet–triplet gap of CH_2. The actual barrier which has to be surmounted is somewhater lower because the energy of the singlet state decreases during the approach of both fragments (Figure 9). From this the energy of the (0,0,0) level of the singlet state decreases with respect to the triplet vibrational levels. For R_{13} = 3.0 Å it lies somewhat above the (0,1,0) level of the triplet state, while an energetic coincidence with the (0,3,0) and (0,2,0) levels of the triplet state has occurred during the CH_2–C_2H_4 approach. Assuming that the vibrational spectra of the singlet and triplet CH_2 species are not changed due to the presence of C_2H_4, the barrier of that path is given by the energy difference between the triplet (0,0,0) level for $R_{13} = \infty$ Å, at which point the reaction starts, and the singlet (0,0,0) level at R_{13} = 3.0 Å. The calculated barrier height of about 6 kcal/mol (Figure 9) is indicated in Figure 10c. Because most secondary geometry parameters change, one has to assume that the perturbations in the vibrational structure increase with further approach of the two fragments which means that the model used above becomes less adequate; i.e. the geometry difference between both states is no longer determined only by the β_3 angle of the CH_2 fragment.

The fourth possibility (Figure 10d) is only given for completeness. The reaction path runs along the triplet surface (TT) to the barrier. The singlet–triplet interconversion occurs at the crossing between TT and SS. Taking the energy into account which is necessary to distort the geometries from TT to TS, the height of the total energy barrier lies around 20 kcal/mol, i.e. nearly twice as high as the energy barriers of the other possibilities.

Summary

In the present work the reactions of $^1CH_2$ and $^3CH_2$ with C_2H_4 have been studied. The minimum energy paths (MEP) of both reactions were calculated, and the different mechanisms were examined. Since the geometry parameters of both reactions differ greatly, the possibility of the participation of the singlet state in the overall reaction starting from the triplet channel had to be studied using various cross sections through both surfaces. It turned out that the energetically favorable conversion from the triplet to the singlet surface can only happen at large CH_2–C_2H_4 separations. Furthermore, it could be shown that if the singlet surface is reached, the consecutive reaction path stays on the singlet surface collapsing to the singlet MEP. To obtain more reliable

data, the barrier height of the pure triplet reaction was examined using more sophisticated treatment than for the parts of the surfaces. The calculations lead to a best estimate of 7–9 kcal/mol. The barrier height of a possible reaction path which starts at the triplet state and interconverts to the singlet state was studied using experimental data of the methylene fragment assuming that at large distances R_{13} its vibrational spectrum is only slightly disturbed by C_2H_4. The upper bound of the barrier height is given by the singlet–triplet splitting of CH_2 (T_e = 9.215 kcal/mol; T_0 = 8.998 kcal/mol[19]), while a lower bound was estimated around 6 kcal/mol. This value lies in the range of the experimental value of 5.3 kcal/mol ($T \approx 600$ K) or about 7 kcal/mol ($T \approx 0$ K),[2] but the uncertainty of the models used in the present study has to be kept in mind.

It is certain that the height of the energy barrier which has to be overcome if the singlet state participates in the reaction processes is comparable to the barrier of the pure triplet reaction.

Acknowledgment. The service and computer time made available by the Computer Center of the University of Bonn are gratefully acknowledged. Part of this work was financially supported by the Deutsche Forschungsgesellschaft (DFG) in the framework of the Leibniz Program.

Registry No. Ethene, 74-85-1; methylene, 2465-56-7.

References and Notes

(1) *Carbenes*; Jones, M., Jr., Moss, R. A., Eds.; Robert E. Kreiger Publishing Co. Inc.: Malabar, FL, 1983; Vols. I and II. *Organic Chemistry*; Kirmese W., Ed.; A Series of Monographs, Vol. I, Carbenes; Academic Press, Inc.: New York, 1971. Jones, M., Jr., Moss, R. A. Carbenes In *Reactive Intermediates*; Jones, M., Jr., Moss, R. A., Eds.; John Wiley & Sons: New York, 1975.
(2) Böhland, T.; Temps, F.; Wagner, H. Gg. *Ber. Bunsen-Ges. Phys. Chem.* **1985**, *89*, 1100. Böhland, T.; Temps, F.; Wagner, H. Gg. *Ber. Bunsen-Ges. Phys. Chem.* **1986**, *90*, 468.
(3) Reuter, W.; Engels, B.; Peyerimhoff, S. D. To be published.
(4) Hoffmann, R. *J. Am. Chem. Soc.* **1968**, *90*, 1475.
(5) Bodor, N.; Dewar, M.; Wasson, J. S. *J. Am. Chem. Soc.* **1972**, *94*, 9095.
(6) Moreno, M.; Lluch, J. M.; Oliva, A.; Bertrán, J. *J. Mol. Struct. (THEOCHEM)* **1988**, *164*, 17.
(7) Siu, A. K. Q.; John, W. M. St.; Hayes, E. F. *J. Am. Chem. Soc.* **1970**, *92*, 7249.
(8) Yamaguchi, K.; Fueno, T. *Chem. Phys. Lett.* **1978**, *53*, 109. Yamaguchi, K.; Fueno, T. *Chem. Phys. Lett.* **1977**, *49*, 555. Yamaguchi, K.; Fueno, T. *Chem. Phys. Lett.* **1973**, *22*, 471.
(9) Kato, S.; Morokuma, K. *Chem. Phys. Lett.* **1979**, *65*, 19.
(10) Yamaguchi, Y.; Osamura, Y.; Schaefer, H. F., III. *J. Am. Chem. Soc.* **1983**, *105*, 7506. Yamaguchi, Y.; Schaefer, H. F., III. *J. Am. Chem. Soc.* **1984**, *106*, 5115.
(11) Goldberg, A. H.; Dougherty, D. A. *J. Am. Chem. Soc.* **1983**, *105*, 284.
(12) Hoffman, R.; Hayes, D. M.; Skell, P. S. *J. Phys. Chem.* **1972**, *76*, 664.
(13) Zurawski, B.; Kutzelnigg, W. *J. Am. Chem. Soc.* **1978**, *100*, 2654.
(14) Huzinaga, S. *J. Chem. Phys.* **1965**, *42*, 1293.
(15) Dunning, T. H. *J. Chem. Phys.* **1970**, *53*, 2823.
(16) Peyerimhoff, S. D.; Buenker, R. J.; Allen, L. C. *J. Chem. Phys.* **1966**, *45*, 734.
(17) Buenker, R. J.; Peyerimhoff, S. D. In *New Horizons in Quantum Chemistry*; Löwdin, P. O., Pullmann, B., Eds.; D. Reidel Publishing Co.: Dodrecht, The Netherlands, 1983.
(18) Bauschlicher, C. W.; Langhoff, S. R.; Taylor, P. R. *J. Chem. Phys.* **1987**, *87*, 387.
(19) Jensen, P.; Bunker, P. R. *J. Chem. Phys.* **1988**, *89*, 1327. Comeau, D. C.; Shavitt, I.; Jensen, P.; Bunker, P. R. *J. Chem. Phys.* **1989**, *90*, 6491. McLean, A. D.; Bunker, P. R.; Escribano, R. M.; Jensen, P. *J. Chem. Phys.* **1987**, *87*, 2166.
(20) Shavitt, I. *Tetrahedron* **1985**, *41*, 1531.
(21) Gdanitz, R. J.; Ahlrichs, R. *Chem. Phys. Lett.* **1988**, *143*, 413. Jenderek, J. Diploma Thesis, Universitat Bonn, Germany, 1990.
(22) Frisch, M. J.; Binkley, J. S.; Schlegel, H. B.; Rhagavachari, K.; Melius, C. F.; Martin, R. L.; Stewart, J. J. P.; Bobrowitz, F. W.; Rohlfing, C. M.; Kahn, L. R.; DeFries, D. J.; Seeger, R.; Whiteside, R. A.; Fox, D. J.; Fluder, E. M.; Pople, J. A. GAUSSIAN 86; Carnegie-Mellon Quantum Chemistry Publishing Unit: Pittsburgh, PA, 1986.
(23) Wagner, H. Gg.; Temps, F. Private communication.
(24) *Landolt-Bornstein*, Neue Serie; Springer-Verlag: Berlin, 1971.
(25) Ortega, M.; Lluch, J. M.; Oliva, A.; Bertran, J. *Can. J. Chem.* **1987**, *65*, 1995.
(26) Koopmans, T. A. *Physica* **1933**, *1*, 104.
(27) Heator, M. M., El-Talbi, M. R. *J. Chem. Phys.* **1986**, *85*, 7198.
(28) Buenker, R. J.; Peyerimhoff, S. D. *Theor. Chim. Acta* **1975**, *35*, 33. Buenker, R. J. *Int. J. Quant. Chem.* **1986**, *29*, 435 and references cited therein.
(29) Kollmar, H. *Tetrahedron Lett.* **1970**, *38*, 3337.
(30) Skell, P. S.; Garner, A. Y. *J. Chem. Phys.* **1956**, *78*, 5430.
(31) Jean, Y.; Chapuisat, X. *J. Am. Chem. Soc.* **1974**, *96*, 6911. Jean, Y.; Chapuisat, X. *J. Am. Chem. Soc.* **1975**, *97*, 6325.

Semiempirical Calculations of Hyperpolarizabilities for Donor–Acceptor Molecules: Comparison to Experiment

Nobuyuki Matsuzawa[†] and David A. Dixon*

The Central Research and Development Department, E. I. Du Pont de Nemours and Co., Inc.,[‡] Experimental Station, P.O. Box 80328, Wilmington, Delaware 19880-0328 *(Received: September 27, 1991)*

The dipole moments (μ), polarizabilities (α), hyperpolarizabilities (β), and second-order hyperpolarizabilities (γ) of benzenes, biphenyls, fluorenes, styrenes, stilbenes, and tolans have been calculated by a finite field method with the PM-3 parametrization of the MNDO Hamiltonian. These results were compared to experimental values obtained from EFISH and THG measurements. Good correlations were obtained, and coefficients between the measured and calculated values (calculated/measured) were 1.11, 0.75, 1.00, and 0.94 for μ, α, β, and γ, respectively. The calculations generally reproduced the dependence of β and γ on the strength of donors and acceptors and the enhancement of β and γ by charge transfer. For each class of compounds, the effect of substituents on the calculated hyperpolarizabilities were studied. Differences between the calculated and measured values were found for certain sets of substituents.

1. Introduction

Nonlinear optical (NLO) effects due to multiphoton processes are being studied for potential applications in various devices, e.g., shortening of the laser wavelength for high-density optical recording and optical switching for optical computing. Examples of NLO effects include second harmonic generation (SHG), third harmonic generation (THG), and the Pockels effect. Organic compounds having extended π-electron systems are one set of candidates for such device applications because of their varied structural features and high nonlinearities.[1]

A variety of measurements are available for the properties of the linear and nonlinear response of bulk materials to an external electric field. Our interest is the prediction of the microscopic

[†] Present address: SONY Corporation Research Center, 174 Fujitsuka-cho, Hodogaya-ku, Yokohama 240, Japan.

0022-3654/92/2096-6232$03.00/0